J|A|C|S COMMUNICATIONS

Published on Web 12/06/2010

Structural Evolution of Zeolitic Imidazolate Framework-8

Surendar R. Venna,[†] Jacek B. Jasinski,[‡] and Moises A. Carreon*,[†]

Department of Chemical Engineering and Conn Center for Renewable Energy Research, University of Louisville, Louisville, Kentucky 40292, United States

Received October 14, 2010; E-mail: macarr15@louisville.edu

Abstract: We report the structural evolution of zeolitic imidazolate framework-8 (ZIF-8) as a function of time at room temperature. We have identified the different stages of ZIF-8 formation (nucleation, crystallization, growth, and stationary periods) and elucidated its kinetics of transformation. We hypothesize that the observed semicrystalline-to-crystalline transformation may take place via solution- and solid-mediated mechanisms, as suggested by the observed phase transformation evolution and Avrami's kinetics, respectively. A fundamental understanding of ZIF-8 structural evolution as demonstrated in this study should facilitate the preparation of functional metal−organic framework phases with controlled crystal size and extent of crystallinity.

Zeolitic imidazolate frameworks (ZIFs),[1] a subclass of metal−organic frameworks (MOFs), have emerged as a novel type of crystalline porous material that combines highly desirable properties of both zeolites and MOFs, such as crystallinity, microporosity, high surface area, and exceptional thermal and chemical stability. In ZIFs, metal atoms such as Zn and Co are linked through N atoms by ditopic imidazolate (Im) or functionalized Im links to form neutral frameworks and provide tunable nanosized pores formed by 4-, 6-, 8-, and 12-membered-ring ZnN_4 and CoN_4 tetrahedral clusters. The framework of ZIF compounds closely resembles the framework of zeolites, i.e., the T−O−T bridges (T = Si, Al, P) in zeolites are replaced by M−Im−M bridges (M = Zn, Co), and coincidentally, the bond angles in both structures are 145°.[1] Emerging functional applications of ZIFs in gas separation,[2] catalysis,[3] and sensing[4] have been recently reported. In particular, ZIF-8 is one of the most studied prototypical ZIF compounds[5] because of its potential functional applications in gas storage, catalysis, and gas separation. ZIF-8 has large pores with diameters of 11.6 Å that are accessible through small apertures with diameters of 3.4 Å, and it has a cubic space group ($I\bar{4}_3m$) with unit cell dimensions of 16.32 Å.

A fundamental understanding on the formation mechanisms of zeolitic imidazolate frameworks is highly important in order to improve structural and morphological control in the synthesis of these novel materials. To the best of our knowledge, almost nothing is known about the nucleation, growth, and crystallization events for this particular type of MOF. Herein, we report the entire process of gel formation, nucleation, crystallization, and growth of ZIF-8 at room temperature.

In a typical synthesis, 0.3 g of zinc nitrate hexahydrate [$Zn(NO_3)_2 \cdot 6H_2O$, Fluka, ≥99%] was dissolved in 11.3 g of methanol (Acros Organics, extra dry, water <50 ppm). A solution consisting of 0.66 g of 2-methylimidazole ($C_4H_6N_2$, Aldrich, 99%) and 11.3 g of methanol was added to the Zn-based solution and vigorously stirred for various times. This gel composition corresponded to that reported previously.[5c,2a] The resultant particles were separated from the gel by centrifugation at 4000 rpm and washed with methanol. This procedure was repeated twice. The resultant ZIF-8 powder was dried overnight at 75 °C.

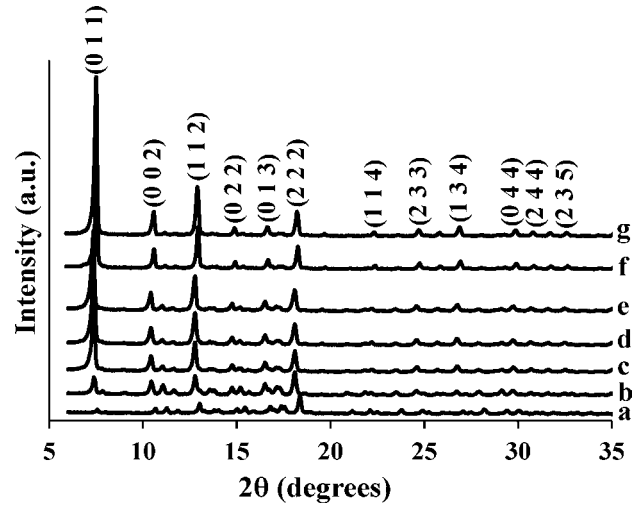

Figure 1. XRD patterns illustrating the structural evolution of ZIF-8 as a function of synthesis time: (a) 20 min; (b) 30 min; (c) 40 min; (d) 50 min; (e) 60 min; (f) 12 h; (g) 24 h.

Powder X-ray diffraction (XRD) patterns were collected using a Bruker D8-Discover diffractometer operating at 40 kV and 40 mA with Cu Kα radiation. Transmission electron microscopy (TEM) images and diffraction patterns were taken using an FEI Tecnai F20 microscope with a field-emission gun operating at an accelerating voltage of 200 kV. ZIF-8 is highly sensitive to the TEM electron beam. For this study, low-dose imaging conditions were employed, using an increased spot size and diverged beam to reduce the radiation damage. The surface area and adsorption−desorption isotherm measurements were carried out on a Micromeritics Tristar 3000 porosimeter at 77 K using liquid nitrogen as the coolant, and the samples were degassed at 135 °C for 3 h before the measurements. The quantitative analysis of elemental carbon, hydrogen, and nitrogen was carried out using a model 440 CHN/O/S analyzer (Exeter Analytical, North Chelmsford, MA).

Figure 1 shows the structural evolution of ZIF-8 as a function of time. For this particular study, ZIF-8 was prepared by reacting zinc nitrate hexahydrate and 2-methylimidazole in the presence of methanol at room temperature. As shown in Figure 1, the most prominent peak for ZIF-8, corresponding to the (011) plane, increased as time progressed. The area under the curve of this peak was quantified using Origin software (after baseline correction) to determine the relative crystallinity of the ZIF-8 phase (Figure S1 and Table S1 in the Supporting Information), which can be related

[†] Department of Chemical Engineering.
[‡] Conn Center for Renewable Energy Research.

 10.1021/ja109268m

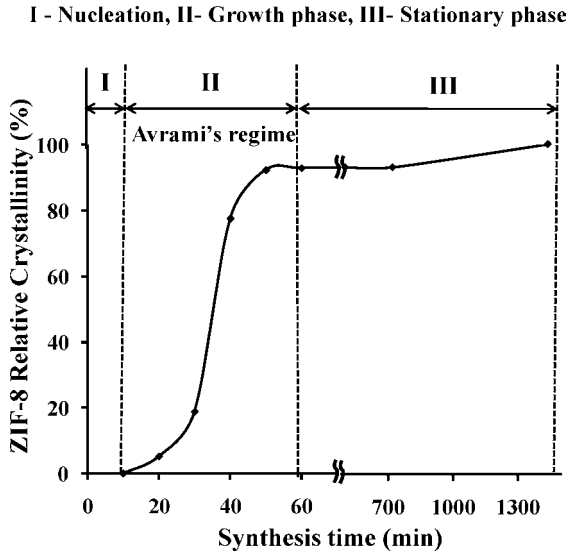

Figure 2. Kinetics of transformation of ZIF-8 as a function of time.

to the phase transformation rate. The presence of sharp peaks even at short synthesis times (20 min) suggests that ZIF-8 likely evolves from a metastable phase. Our group[6a] and others[6b,c] have used similar analyses to determine the relative amounts of phases/crystallinity in porous frameworks. As shown in Figure 1, the relative crystallinity of ZIF-8 increases slowly at short synthesis times. Next, a rapid increase is observed in the 30−40 min range. Finally, after 50 min, the relative crystallinity of ZIF-8 remained practically constant (above 90%), reaching a maximum of 100% at 24 h. Since longer synthesis times (48 h) did not change the area under the curve of the (011) peak of ZIF-8 in comparison to the 24 h sample, it is reasonable to assume that the ZIF-8 relative crystallinity achieves its maximum at 24 h. It is important to mention that small particles were observed at 10 min, but due to the extremely small yield, we were not able to record their XRD pattern. Nevertheless, TEM revealed that ∼50 nm particles, some of them already faceted, evolved at 10 min.

As shown in Figure 2, the structural evolution of ZIF-8 as a function of time can be divided into three stages. Initially ($t < 10$ min), there is an incubation time required to nucleate the ZIF-8 phase, corresponding to the nucleation stage (I). After nucleation, there is a growth stage (II) during which the relative crystallinity of ZIF-8 increases with time. In this region, a maximum in crystallinity is achieved at ∼60 min. Interestingly, in this sigmoidal regime, the kinetics of transformation followed Avrami's classical model;[7] therefore, the relative crystallinity of ZIF-8 as a function of time in this region can be expressed as $y = 1 - \exp(-kt^n)$, where k is a scaling constant and n is the Avrami constant. For our case, $k = 5.1 \times 10^{-7}$ and $n \approx 4$, as shown in Figure S2. In particular, n gives useful information regarding the nucleation process and the shape of the growing entities. Typically, an n value of 4 suggests that the phase nucleates randomly in the parent phase (homogeneous nucleation) and that the growing entities adopt spherical shapes.[8] Finally, in the stationary phase (III, $t > 60$ min), the ZIF-8 relative crystallization rate remains relatively constant as the metastable phase is consumed. Time-resolved in situ energy-dispersive XRD (EDXRD) was recently used to follow the crystallization of the transition-metal carboxylate MOFs HKUST-1 and MIL-53.[9] Interestingly, the kinetics of crystallization for HKUST-1 followed the Avrami−Erofe'ev model.

The solution pH was also followed as a function of synthesis time. The initial pH of the solution was 7.8. The pH decreased to

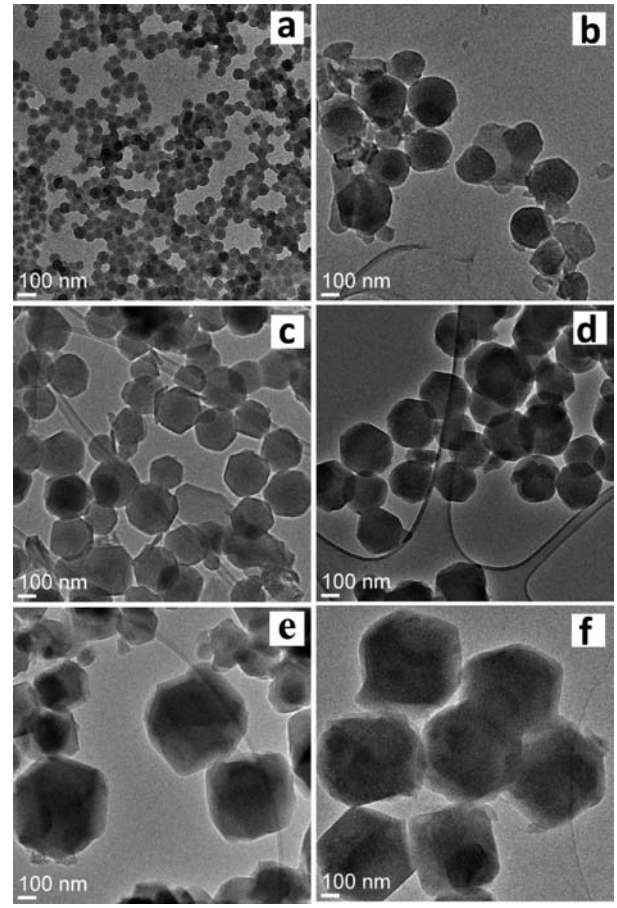

Figure 3. TEM images of ZIF-8 as a function of synthesis time: (a) 10 min; (b) 30 min; (c) 40 min; (d) 60 min; (e) 12 h; (f) 24 h.

7.5, 7.4, and 7.3 at 10, 20, and 40 min, respectively. At 50 min and later, the pH remained practically constant at 7.2 (Figure S3). These pH changes correlated with the changes in ZIF-8 relative crystallinity, suggesting that a reduction in the pH may promote the crystallization of the framework. At equilibrium, protonated and neutral forms of the imidazole linker coexist in solution.[5c] On the basis of the correlation between the solution pH and the evolution of the ZIF-8 relative crystallinity, it is likely that the concentration of the deprotonated linker decreases as pH decreases, resulting in the stabilization of the neutral form of the linker, which ultimately limits the rate of phase transformation, as confirmed by the late stages of Avrami's regime and the stationary region of Figure 2. Studies based on pH behavior in methanol-based solutions for the synthesis of ZIF-8 have been reported by independent groups.[2g,5c]

The formation and growth of ZIF-8 was confirmed by TEM images, as shown in Figure 3. The sample synthesized at 10 min exhibited ∼50 nm spherical (consistent with Avrami's model) and faceted particles displaying a narrow size distribution. The presence of some faceted particles indicates the initial stages of crystallization. At 30 min, the particle size increased to 230 ± 40 nm (Figure 3b). Furthermore, some crystals showed facets. As shown in Figure 3c,d, the size of the crystals remained practically constant at 40 and 60 min; however more homogeneous faceted crystals were observed. In particular, 230 ± 20 nm homogeneous crystals were observed at 60 min. At 12 h, the crystal size increased to 500 ± 40 nm and became less homogeneous (Figure 3e). Finally, Figure 3f shows ∼500 nm crystals displaying a relatively narrow size distribution. The TEM images revealed that as the crystallization

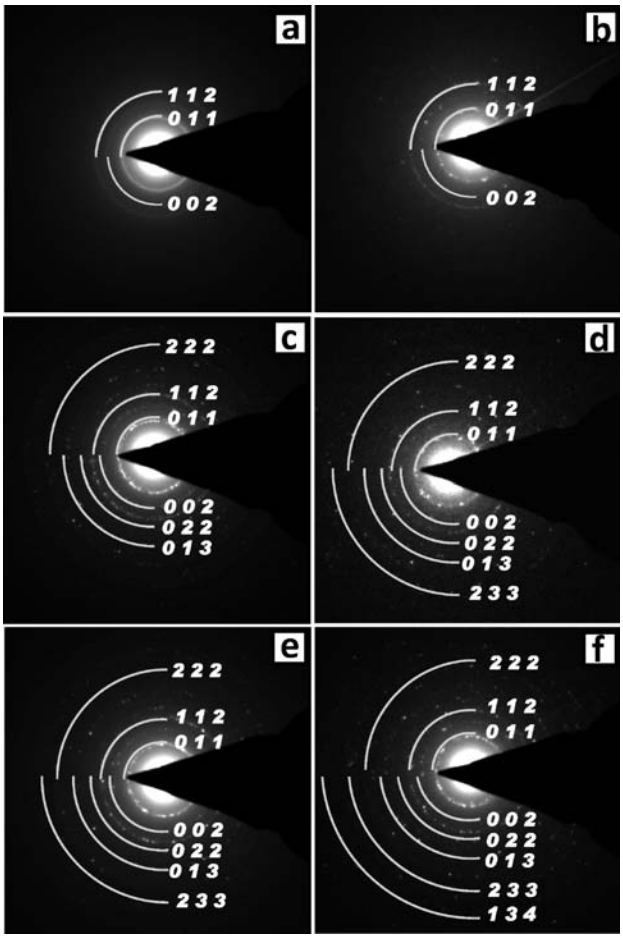

Figure 4. SAED ring patterns of ZIF-8 as a function of synthesis time: (a) 10 min; (b) 30 min; (c) 40 min; (d) 60 min; (e) 12 h; (f) 24 h.

time increased from 10 min to 24 h, the average particle size increased significantly, most likely as a result of Ostwald ripening. In this spontaneous, thermodynamically driven process, small particles disappear at the expense of growing larger ones, which are energetically favored.

Figure 4 shows the selected-area electron diffraction (SAED) patterns as a function of synthesis time. As shown in Figure 4a, the start of the formation of crystal planes of ZIF-8 was observed. The well-defined ring nature of the SAED pattern confirmed the formation of crystallites of ZIF-8. Because of the relatively small crystallite size, the rings were diffuse. As the synthesis time increased, the average crystal size increased, and the SAED rings became more "spotty". The *d* spacing of the (011) plane calculated from the SAED patterns is ~11.95 Å, in agreement with the value obtained from the XRD pattern as well as reported values of the *d* spacing for crystalline ZIF-8 particles.[2a] The cubic lattice parameter of these crystals is 16.87 Å.

Figure 5 shows single-crystal SAED patterns from a few randomly selected crystals of sample synthesized for 12 h. All of these patterns were consistently indexed using a bcc crystal structure. Moreover, the lattice parameter obtained from these patterns agrees with the one expected for ZIF-8 within the experimental error.

The nitrogen adsorption−desorption isotherms displayed type-I behavior, which is typical of microporous phases (Figure S4). Interestingly, the specific Brunauer−Emmett−Teller (BET) surface areas correlated with the ZIF-8 relative crystallinity (i.e., the observed surface area was low at 20 and 30 min, increased rapidly

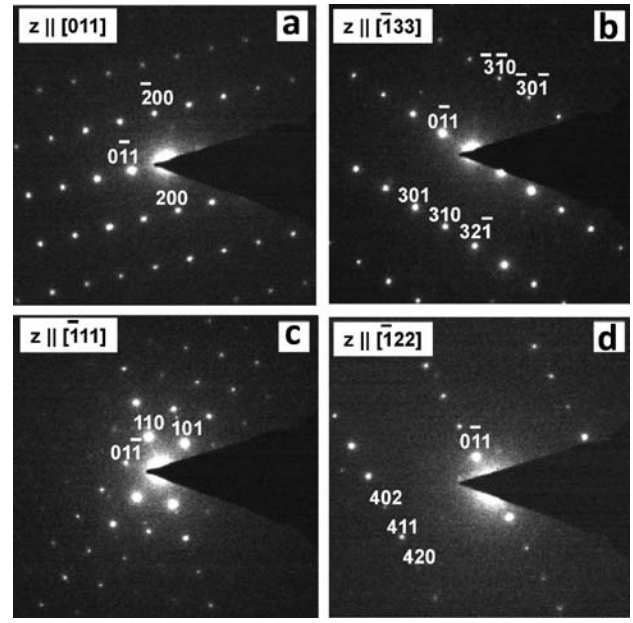

Figure 5. SAED patterns of ZIF-8 crystals synthesized at 12 h taken from four crystals oriented close to the (a) [011], (b) [1̄33], (c) [1̄11], and (d) [1̄22] zone axes, respectively. The indexing of the patterns is consistent with the bcc crystal structure of ZIF-8.

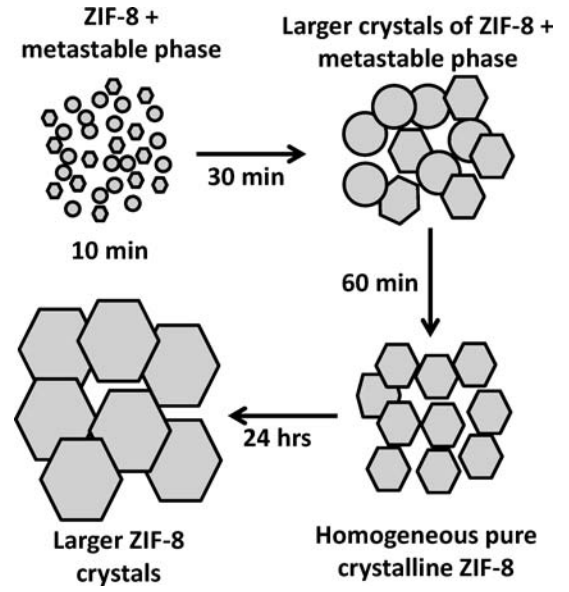

Figure 6. Proposed formation pathway of ZIF-8 as a function of synthesis time.

in the 40−60 min range, and remained practically constant after 60 min, as shown in Table S2). The CHN analysis of the crystalline ZIF-8 sample showed that the percentages of these elements were C 41.11, H 4.62, and N 24.86 (ash 26.5), in close agreement with the theoretical values.[5c]

Figure 6 shows a schematic illustration of the potential events that may take place during the formation of ZIF-8 crystals. Our XRD analysis and TEM studies support the proposed formation pathway. The homogenized gel solution leads to ~50 nm particles after 10 min. From in situ light scattering studies, Cravillon et al.[5c] concluded that there is simultaneous ZIF-8 seed formation and fast crystal growth on a time scale of a few seconds. As time progresses, tiny ZIF-8 crystallites grow at the expense of the surrounding spherical gel agglomerates, most likely as a result of supersaturation

within the gel particles. This phenomenon has been observed during the formation of various types of zeolites, including zeolites A,[10a] Y,[10b] and Si-MFI.[10c,d] At this point, ZIF-8 and a metastable phase coexist. The fraction of ZIF-8 phase increases until the nutrient pool (the remaining metastable phase) is totally exhausted, leading to a fully crystalline ZIF-8 phase. On the basis of the XRD analysis, one may assume that the ZIF-8 structure is fully developed at synthesis times longer than 50 min. Finally, to attain a lower energy state, the "small" crystals need to transform into "larger" crystals via the Ostwald ripening mechanism.[11]

As suggested for several zeolite systems,[12] the medium-range order (low relative crystallinity) observed in ZIF-8 may be related to weak van der Waals intermolecular interactions established in the synthesis gel before the development of long-range order of the crystal, leading to the fully crystalline phase. This strongly suggests that species in solution participating in the formation of the ZIF-8 may form a structure with medium-range order and then develop long-range order by solution-transport or solid-state (supported by Avrami's kinetics) transformation mechanisms or by a combination of the two.

In summary, we have followed the structural evolution of ZIF-8 as a function of time at room temperature. We have identified the different stages of ZIF-8 formation (nucleation, crystallization, growth, and stationary periods) and elucidated its kinetics of transformation. We hypothesize that the observed semicrystalline-to-crystalline transformation may take place via solution- and solid-mediated mechanisms, as suggested by the observed phase transformation evolution and Avrami's kinetics, respectively. We have found that the reduction in solution pH plays an important role as the driving force for the crystallization process. A fundamental understanding of ZIF-8 structural evolution as demonstrated in this study should facilitate the preparation of novel functional materials. For instance, we are currently growing ZIF-8 membranes to be used for molecular separations at different synthesis times, which in principle will allow us to effectively control the crystal size and membrane thickness, which are critical parameters in the preparation of efficient membranes.

Acknowledgment. This work was partially supported by an ACS-PRF grant (# 49202-DNI5).

Supporting Information Available: Calculation of ZIF-8 relative crystallinity, Avrami's analysis, solution pH as a function of synthesis time, and nitrogen adsorption−desorption isotherms. This material is available free of charge via the Internet at http://pubs.acs.org.

References

(1) (a) Hayashi, H.; Côte, A. P.; Furukawa, H.; O'Keeffe, M.; Yaghi, O. M. *Nat. Mater.* **2007**, *6*, 501. (b) Banerjee, R.; Phan, A.; Wang, B.; Knobler, C.; Furukawa, H.; O'Keeffe, M. *Science* **2008**, *319*, 939. (c) Wang, B.; Côte, A. P.; Furukawa, H.; O'Keeffe, M.; Yaghi, O. M. *Nature* **2008**, *453*, 207. (d) Morris, W.; Doonan, C. J.; Furukawa, H.; Banerjee, R.; Yaghi, O. M. *J. Am. Chem. Soc.* **2008**, *130*, 12626. (e) Banerjee, R.; Furukawa, H.; Britt, D.; Knobler, C.; O'Keeffe, M.; Yaghi, O. M. *J. Am. Chem. Soc.* **2009**, *131*, 3875. (f) Phan, A.; Doonan, C. J.; Uribe-Romo, F. J.; Knobler, C. B.; O'Keeffe, M.; Yaghi, O. M. *Acc. Chem. Res.* **2010**, *43*, 58.

(2) (a) Venna, S. R.; Carreon, M. A. *J. Am. Chem. Soc.* **2010**, *132*, 76. (b) Bux, H.; Liang, F.; Li, Y.; Cravillon, J.; Wiebcke, M.; Caro, J. *J. Am. Chem. Soc.* **2009**, *131*, 16000. (c) Liu, Y.; Hu, E.; Khan, E. A.; Lai, Z. *J. Membr. Sci.* **2010**, *353*, 36. (d) Huang, A.; Bux, H.; Steinbach, F.; Caro, J. *Angew. Chem., Int. Ed.* **2010**, *49*, 4958. (e) Li, Y.; Liang, F.; Bux, H.; Yang, W.; Caro, J. *J. Membr. Sci.* **2010**, *354*, 48. (f) Li, Y.; Bux, H.; Feldhoff, A.; Li, G.; Yang, W.; Caro, J. *Adv. Mater.* **2010**, *22*, 3322. (g) McCarthy, M. C.; Varela-Guerrero, V.; Barnett, G. V.; Jeong, H.-K. *Langmuir* **2010**, *26*, 14636.

(3) Jiang, H. L.; Liu, B.; Akita, T.; Haruta, M.; Sakurai, H.; Xu, Q. *J. Am. Chem. Soc.* **2009**, *131*, 11302.

(4) Lu, G.; Hupp, J. T. *J. Am. Chem. Soc.* **2010**, *132*, 7832.

(5) (a) Huang, X.-C.; Lin, Y.-Y.; Zhang, J.-P.; Chen, X.-M. *Angew. Chem., Int. Ed.* **2006**, *45*, 1557. (b) Park, K. S.; Ni, Z.; Côté, A. P.; Choi, J. Y.; Huang, R.; Uribe-Romo, F. J.; Chae, H. K.; O'Keeffe, M.; Yaghi, O. M. *Proc. Natl. Acad. Sci. U.S.A.* **2006**, *103*, 10186. (c) Cravillon, J.; Muzer, S.; Lohmeier, S. J.; Feldhoff, A.; Huber, K.; Wiebcke, M. *Chem. Mater.* **2009**, *21*, 1410.

(6) (a) Venna, S. R.; Carreon, M. A. *J. Mater. Chem.* **2009**, *19*, 3138. (b) Choi, S. Y.; Mamak, M.; Speakman, S.; Chopra, N.; Ozin, G. A. *Small* **2005**, *1*, 226. (c) Choi, S. Y.; Lee, B.; Carew, D. B.; Mamak, M.; Peiris, F. C.; Speakman, S.; Chopra, N.; Ozin, G. A. *Adv. Funct. Mater.* **2006**, *16*, 1731.

(7) (a) Avrami, M. *J. Chem. Phys.* **1939**, *7*, 1103. (b) Avrami, M. *J. Chem. Phys.* **1940**, *8*, 212. (c) Avrami, M. *J. Chem. Phys.* **1941**, *9*, 177.

(8) (a) Hillier, I. H. *J. Polym. Sci., Part A* **1965**, *3*, 3067. (b) Hay, J. N. *J. Polym. Sci., Polym. Lett. Ed.* **1976**, *14*, 543.

(9) Millange, F.; Medina, M. I.; Guillou, N.; Férey, G.; Golden, K. M.; Walton, R. I. *Angew. Chem. Int. Ed.* **2010**, *49*, 763.

(10) (a) Mintova, S.; Olson, N. H.; Valtchev, V.; Bein, T. *Science* **1999**, *283*, 958. (b) Mintova, S.; Olson, N. H.; Bein, T. *Angew. Chem., Int. Ed.* **1999**, *38*, 3201. (c) Mintova, S.; Olson, N. H.; Senker, J.; Bein, T. *Angew. Chem., Int. Ed.* **2002**, *41*, 2558. (d) Burkett, S. L.; Davis, M. E. *J. Phys. Chem.* **1994**, *98*, 4647.

(11) Ratke, L.; Voorhees, P. W. *Growth and Coarsening: Ripening in Material Processing*; Springer: Berlin, 2002; p 117.

(12) Davis, M. E.; Lobo, R. F. *Chem. Mater.* **1992**, *4*, 756.

JA109268M